

# Phase structure of a holographic topological superconductor beyond the probe limit

Hoang Van Quyet<sup>a</sup>,

<sup>a</sup>*Department of Physics Hanoi Pedagogical University 2 Xuan Hoa Phu Tho Vietnam*

---

## Abstract

We investigate the phase structure and tricritical behavior of a holographic topological superconductor model using Einstein-Maxwell gravity in Anti-de Sitter spacetime. By incorporating both gravitational backreaction ( $\kappa^2 = 1$ ) and a quartic self-interaction term  $V(\phi) = \lambda\phi^4$ , we demonstrate that this self-interaction not only is essential for the existence of a tricritical point (TCP) separating second-order and first-order phase transitions, but also actively controls its location in the phase diagram. For a representative coupling  $\tilde{\lambda} = 0.1$ , the TCP is located at  $(q_{\text{tri}}, T_{\text{tri}}) = (2.00 \pm 0.02, 0.1521 \pm 0.0003)$  in the  $(q, T)$  parameter space. The backreacted critical temperature shows an enhancement by a factor of approximately 1.22 compared to the probe limit. Crucially, the tricritical scaling analysis yields an exponent  $\phi \approx 0.67$ , which is in excellent agreement with the mean-field prediction  $\phi = 2/3$ . This result confirms that while gravitational backreaction shifts the critical points and modifies the phase diagram topology, it does not alter the universality class of the phase transition in the large- $N$  limit. The order parameter critical exponent  $\beta \approx 0.50$  also remains consistent with mean-field theory. The frequency-dependent conductivity exhibits a superconducting gap with energy ratio  $\omega_g/T_c = 3.18 \pm 0.05$ . Holographic entanglement entropy confirms the orders of the phase transitions. Our thermodynamic analysis employs proper holographic renormalization to ensure finite and non-vanishing free energy for the normal phase, with clear swallowtail structure demonstrating first-order phase transitions.

*Keywords:* Holographic superconductor, AdS/CFT correspondence, Tricritical point, Gravitational backreaction, Phase transition, Scaling laws

---

## 1. Introduction

The gauge/gravity duality, also known as the Anti-de Sitter (AdS)/conformal field theory (CFT) correspondence, provides a powerful framework for studying strongly coupled quantum field theories (QFTs) by mapping them to weakly coupled classical gravity theories in one higher dimension [1, 2, 3, 4]. This duality has found numerous applications in condensed matter physics, particularly in understanding phenomena like high-temperature superconductivity, which are notoriously difficult to analyze using conventional perturbative methods.

---

*Email address:* hoangvanquyet@hpu2.edu.vn (Hoang Van Quyet)

In this context, the concept of a “holographic superconductor” was introduced, modeling a  $(2+1)$ -dimensional superconductor as the boundary theory of a  $(3+1)$ -dimensional gravitational system, typically involving a charged scalar field coupled to a Maxwell field in an AdS-black hole background [5, 6, 7]. The condensation of the scalar field in the bulk gravity theory corresponds to the formation of a superconducting condensate in the boundary QFT, occurring below a critical temperature  $T_c$ .

Various types of holographic superconductors have been constructed, including  $s$ -wave [6, 8, 9],  $p$ -wave [8, 9], and  $d$ -wave models [10], corresponding to different operator dimensions and symmetries of the condensate.

Recently, topological superconductors (TSCs) have attracted significant attention due to their potential applications in fault-tolerant quantum computation, attributed to the presence of robust Majorana zero modes [11]. Consequently, constructing holographic models of topological superconductors has become an active area of research, aiming to provide insights into the strongly coupled nature of these exotic states.

Most holographic superconductor models are initially studied in the probe limit ( $e^2 \rightarrow \infty$  or  $G \rightarrow 0$ ), where the backreaction of the matter fields on the background spacetime geometry is neglected. This simplification is computationally convenient but ignores important strong coupling effects. To explore physics beyond the probe limit, one must consider the gravitational backreaction, quantified by the gravitational coupling  $\kappa^2 = 16\pi G$ . The influence of backreaction has been shown to quantitatively (and sometimes qualitatively) modify the phase structure [12, 13, 14, 15, 16, 17, 18, 19, 20]. On the other hand, the quartic self-interaction  $V(\phi) = \lambda\phi^4$  is also crucial. It was shown that this term is required for the existence of first-order phase transitions and, consequently, tricritical points in certain holographic models [21, 22, 23, 24, 25].

While the combined effects of backreaction and self-interaction have been explored, a systematic study of their interplay in establishing the tricritical phase structure is still lacking. Specifically, the self-interaction coupling  $\lambda$  is often treated merely as a fixed parameter necessary for the transition, rather than an active component of the phase diagram. Furthermore, the precise values of critical exponents at a fully backreacted tricritical point are not well-established.

In this paper, we investigate the phase structure of a holographic topological superconductor model, systematically incorporating the combined effects of gravitational backreaction and the quartic self-interaction. We aim to find and analyze the tricritical point (TCP) where the phase transition changes from second to first order. A primary goal of this work is to address the crucial role of the self-interaction, demonstrating not only that  $\lambda$  is essential for the TCP’s existence, but also showing how it quantitatively controls the TCP’s location by mapping the phase diagram’s dependence on  $\lambda$ . We will also study the tricritical scaling exponents governing the behavior near the TCP. We find a tricritical exponent  $\phi \approx 0.67$ , which is in excellent agreement with the mean-field value  $\phi = 2/3$ . This agreement confirms that the universality class of the phase transition remains robust under strong backreaction effects. Finally, we compute the frequency-dependent conductivity to determine the superconducting gap ratio  $\omega_g/T_c$  and use holographic entanglement entropy to further probe the thermodynamic nature of the phase transitions.

The thermodynamic analysis presented in this work addresses a critical technical point that ensures the physical correctness of our results. In particular, we employ the full machin-

ery of holographic renormalization [26, 27, 28] to compute the grand potential (free energy) of both the normal and superconducting phases. This approach guarantees that the free energy of the normal phase (corresponding to the RN-AdS black hole) is correctly finite and non-vanishing, as required by the proper regularization of the on-shell action with appropriate boundary terms including the Gibbons-Hawking term and counterterms. The resulting free energy landscape clearly exhibits the characteristic swallowtail structure that serves as the definitive thermodynamic signature of first-order phase transitions in holographic systems.

The paper is organized as follows. In section 2, we introduce the holographic model and derive the equations of motion. In section 3, we outline the numerical methods used to solve the coupled differential equations. In section 4, we present the main results for the phase diagram, including the identification of the tricritical point and the new results on its  $\lambda$ -dependence. In section 5, we perform the tricritical scaling analysis and discuss the agreement with mean-field predictions. section 6 is devoted to the calculation of conductivity. section 7 investigates the entanglement entropy. We conclude with a summary and discussion of our results in section 7.

## 2. Holographic Model

### 2.1. Action and Equations of Motion

We consider a  $(3+1)$ -dimensional holographic model of a topological superconductor, described by Einstein-Maxwell gravity coupled to a charged scalar field with a quartic self-interaction term. The action in  $(3+1)$ -dimensional Anti-de Sitter (AdS) spacetime is given by:

$$S = \int d^4x \sqrt{-g} \left[ \frac{1}{2\kappa^2} \left( R + \frac{6}{L^2} \right) - \frac{1}{4} F_{\mu\nu} F^{\mu\nu} - |D_\mu \phi|^2 - V(\phi) \right], \quad (1)$$

where  $R$  is the Ricci scalar,  $F_{\mu\nu} = \nabla_\mu A_\nu - \nabla_\nu A_\mu$  is the Maxwell field strength tensor, and  $A_\mu$  is the gauge field. The covariant derivative is defined as  $D_\mu \phi = \nabla_\mu \phi - iqA_\mu \phi$ , where  $q$  is the charge of the scalar field. The gravitational coupling constant is  $\kappa^2 = 16\pi G$ , where  $G$  is the four-dimensional Newton constant, and  $L$  is the AdS radius (set to  $L = 1$  hereafter). To incorporate the gravitational backreaction, which is a central part of this study, we fix the coupling constant  $\kappa^2 = 1$  throughout this work. This choice places the model in a strong backreaction regime.

The scalar field  $\phi$  with mass  $m$  and charge  $q$  is minimally coupled to the gauge field  $A_\mu$ . The potential  $V(\phi) = -m^2\phi^2 + \lambda\phi^4$  includes both a mass term and the quartic self-interaction, with  $\lambda > 0$  ensuring the potential is bounded from below. We work in the parameter regime where  $m^2L^2 = -2$ , corresponding to a boundary operator of dimension  $\Delta = 2$ .

By varying the action with respect to the metric  $g_{\mu\nu}$ , the gauge field  $A_\mu$ , and the scalar field  $\phi$ , we obtain the Einstein equation, Maxwell equation, and Klein-Gordon equation, respectively:

$$R_{\mu\nu} - \frac{1}{2}g_{\mu\nu}R - 3g_{\mu\nu} = \kappa^2 T_{\mu\nu}^{(m)}, \quad (2)$$

$$\nabla_\mu F^{\mu\nu} = J^\nu, \quad (3)$$

$$(\nabla_\mu - iqA_\mu)(\nabla^\mu - iqA^\mu)\phi - m^2\phi - 2\lambda\phi^3 = 0, \quad (4)$$

where the energy-momentum tensor  $T_{\mu\nu}^{(m)}$  and the current  $J^\nu$  are given by:

$$T_{\mu\nu}^{(m)} = F_{\mu\rho}F_\nu^\rho - \frac{1}{4}g_{\mu\nu}F_{\rho\sigma}F^{\rho\sigma} \quad (5)$$

$$+ (\nabla_\mu + iqA_\mu)\phi^\dagger(\nabla_\nu - iqA_\nu)\phi + (\nabla_\nu + iqA_\nu)\phi^\dagger(\nabla_\mu - iqA_\mu)\phi \quad (6)$$

$$- g_{\mu\nu}\mathcal{L}_m, \quad (7)$$

$$J^\nu = iq[\phi^\dagger(\nabla^\nu - iqA^\nu)\phi - \phi(\nabla^\nu + iqA^\nu)\phi^\dagger], \quad (8)$$

where  $\mathcal{L}_m = -\frac{1}{4}F_{\mu\nu}F^{\mu\nu} - |D_\mu\phi|^2 - V(\phi)$  is the matter Lagrangian density.

The Hawking temperature of the black hole is given by:

$$T = \frac{1}{4\pi} \left( \frac{f'(z)}{e^{-\chi(z)/2}} \right)_{z=z_h}, \quad (9)$$

where the prime denotes derivative with respect to  $z$ , and  $z_h$  is the horizon position defined by  $f(z_h) = 0$ .

## 2.2. Dimensionless Parameters and Ansätze

We work with a planar AdS black hole background. The metric ansatz that respects the boundary symmetries is:

$$ds^2 = \frac{1}{z^2} \left( -f(z)e^{-\chi(z)}dt^2 + \frac{dz^2}{f(z)} + dx^2 + dy^2 \right), \quad (10)$$

where  $z = 1/r$  is the radial coordinate. The AdS boundary is at  $z = 0$ , and the black hole horizon  $z_h$  is defined by  $f(z_h) = 0$ . We look for solutions with a non-trivial scalar field  $\phi(z)$  and an electrostatic potential  $A_t(z)$  (in the  $A_z = 0$  gauge):

$$\phi = \phi(z), \quad A_t = A_t(z). \quad (11)$$

To simplify the equations, we introduce dimensionless quantities by scaling with the chemical potential  $\mu$ :

$$z \rightarrow z/z_h, \quad T \rightarrow T/\mu, \quad q \rightarrow q. \quad (12)$$

We define dimensionless parameters:

$$\tilde{T} = \frac{T}{\mu}, \quad \tilde{q} = \frac{q}{\mu}, \quad \tilde{m}^2 = m^2L^2, \quad \tilde{\lambda} = \lambda L^2. \quad (13)$$

In this paper, we work in the parameter regime  $\tilde{m}^2 = -2$  (corresponding to a boundary operator of dimension  $\Delta = 2$ ) and set  $\tilde{\mu} = 1$  (which implies  $q = \tilde{q}$  and  $T = \tilde{T}$ ). We primarily

focus on a representative coupling  $\tilde{\lambda} = 0.1$  for a detailed analysis of the phase structure and critical exponents. However, to elucidate the crucial role of the self-interaction in establishing the tricritical behavior, we will also systematically investigate the dependence of the phase diagram on  $\tilde{\lambda}$  in section 4.

The resulting system of differential equations consists of coupled equations for the functions  $\phi(z)$ ,  $A_t(z)$ ,  $f(z)$ , and  $\chi(z)$ . These equations are solved numerically with appropriate boundary conditions at the horizon  $z_h$  and the AdS boundary  $z = 0$ . The phase structure is then investigated in the  $(q, T)$  plane.

### 3. Numerical Implementation and Convergence Analysis

#### 3.1. Computational Methodology

Our numerical approach employs a sophisticated adaptive shooting method to solve the stiff system of coupled differential equations [29]. The algorithm proceeds through the following steps:

1. **Horizon regularization:** Near  $r = r_h$ , we implement series expansions ensuring regularity:  $\phi(r_h) = 0$  and  $\phi'(r_h) = \phi_0 \cdot g(r_h)$  where  $g(r_h)$  depends on the local geometry.
2. **Adaptive integration:** We employ a fourth-order Runge-Kutta integration scheme with dynamically adjusted step sizes  $\Delta r \in [10^{-5}, 10^{-3}]$ , automatically refined in regions of rapid field variation.
3. **Boundary matching:** At the AdS cutoff  $r_{\max}$ , we impose asymptotic boundary conditions and extract physical quantities through holographic renormalization.
4. **Newton-Raphson iteration:** The shooting parameters are optimized using Newton-Raphson methods with a convergence criterion  $< 10^{-12}$ .

To observe the characteristic “swallowtail” structure of first-order phase transitions, we have improved the algorithm to scan the entire parameter space of initial conditions at the event horizon. In the first-order phase transition region, for a fixed temperature  $T$  value, there exist multiple solutions corresponding to different values of the order parameter  $\langle \mathcal{O} \rangle$ . The algorithm is designed to capture the stable, metastable, and unstable solution branches, ensuring that the multivalued structure of the free energy is accurately reproduced.

This enhancement is crucial for correctly reproducing the thermodynamic behavior near first-order phase transitions. In the free energy analysis, we must include all solution branches to properly identify the global minimum and determine the stable phase of the system.

The computation of the free energy requires special attention to the proper regularization of the on-shell action. The Euclidean on-shell action  $S_{\text{on-shell}}$  diverges at the asymptotic boundary due to the infinite volume of AdS space. To obtain a physically finite quantity, we must supplement it with the Gibbons-Hawking boundary term and counterterms derived from holographic renormalization [26, 27, 28]. The grand potential  $\Omega$  is then given by:

$$\Omega = T(S_{\text{on-shell}} + S_{\text{GH}} + S_{\text{ct}}) , \quad (14)$$

where the Gibbons-Hawking term is:

$$S_{\text{GH}} = -2 \int_{\partial\mathcal{M}} d^3x \sqrt{-\gamma} K , \quad (15)$$

and the counterterms are chosen to cancel the UV divergences:

$$S_{\text{ct}} = \int_{r \rightarrow \infty} d^3x \sqrt{-\gamma} \left( \frac{2}{L} + \frac{L}{2} R[\gamma] - \frac{L}{2} \phi^2 \right). \quad (16)$$

Here  $\gamma$  is the induced metric on the boundary,  $K$  is the extrinsic curvature of the boundary, and  $R[\gamma]$  is the Ricci scalar of the induced metric. The inclusion of this complete set of terms is essential for the free energy to be well-defined and comparable between phases.

It is particularly important to note that with this proper regularization, the free energy of the normal phase (RN-AdS black hole) is finite and non-vanishing. The common misconception that the normal phase free energy vanishes is incorrect and would lead to unphysical thermodynamic conclusions. Our calculation shows that  $\Omega_{\text{normal}}$  takes a specific finite value that serves as the reference against which the superconducting phase condensation energy is measured.

Specifically, the renormalized grand potential for the normal phase is:

$$\Omega_{\text{normal}} = -\frac{1}{2\kappa^2} \left( \frac{f'(z)}{z^2 e^{\chi(z)/2}} \right)_{z \rightarrow 0} + \Omega_{\text{ct}}, \quad (17)$$

where  $\Omega_{\text{ct}}$  includes the finite contributions from the counterterms. The difference  $\Delta\Omega = \Omega_{\text{SC}} - \Omega_{\text{normal}}$  then provides the physically meaningful condensation energy that determines the stability of competing phases.

In our analysis, we plot  $\Delta\Omega = \Omega_{\text{SC}} - \Omega_{\text{RN}}$  as a function of temperature, where  $\Omega_{\text{RN}}$  denotes the grand potential of the Reissner-Nordström-AdS (RN-AdS) black hole (normal phase), while  $\Omega_{\text{SC}}$  corresponds to the superconducting phase. This difference clearly shows the condensation energy gain and enables the identification of phase transitions.

### 3.2. Convergence and Error Analysis

We performed systematic convergence tests to ensure numerical reliability. Table 1 demonstrates that critical temperatures stabilize for  $r_{\text{max}} \geq 50$ , which we adopt for all calculations.

$r_{\text{max}}$	$T_c$ (Second-order)	$T_c$ (First-order)
30	0.1523	0.1489
40	0.1521	0.1487
50	0.1521	0.1487
60	0.1521	0.1487

Table 1: Dependence of the critical temperature  $T_c$  on the AdS cutoff radius  $r_{\text{max}}$ . Results are shown for both second-order and first-order transition cases. The values stabilize for  $r_{\text{max}} \geq 50$ , indicating numerical convergence.

Critical temperatures are determined with precision  $\Delta T/T \sim 10^{-4}$  through systematic bisection methods. The tricritical point location is determined as:

$$(q_{\text{tri}}, T_{\text{tri}}) = (2.00 \pm 0.02, 0.1521 \pm 0.0003). \quad (18)$$

Error bars are estimated through Monte Carlo sampling of initial conditions and systematic variation of numerical parameters.

To verify the numerical reliability of our scaling exponent results, we performed a separate convergence test on the tricritical exponent  $\phi$ . We explicitly verified that the resulting exponent  $\phi \approx 0.67$  is robust against further refinement of the grid spacing  $\Delta r$ . Halving the typical step size did not produce any significant deviation in the fitted exponent. This confirms that the excellent agreement with the mean-field value is a genuine physical prediction of the model, not a finite-size artifact of the numerical discretization.

## 4. Phase Structure

### 4.1. Phase Diagram and Tricritical Point

We first map out the phase diagram in the  $(q, T)$  plane. The critical temperature  $T_c$  is determined by finding the non-trivial solutions ( $\phi_2 \neq 0$ ) at the boundary  $\phi_1 = 0$ . The resulting phase diagram for a fixed representative coupling  $\tilde{\lambda} = 0.1$  and  $\kappa^2 = 1$  is shown in fig. 1.

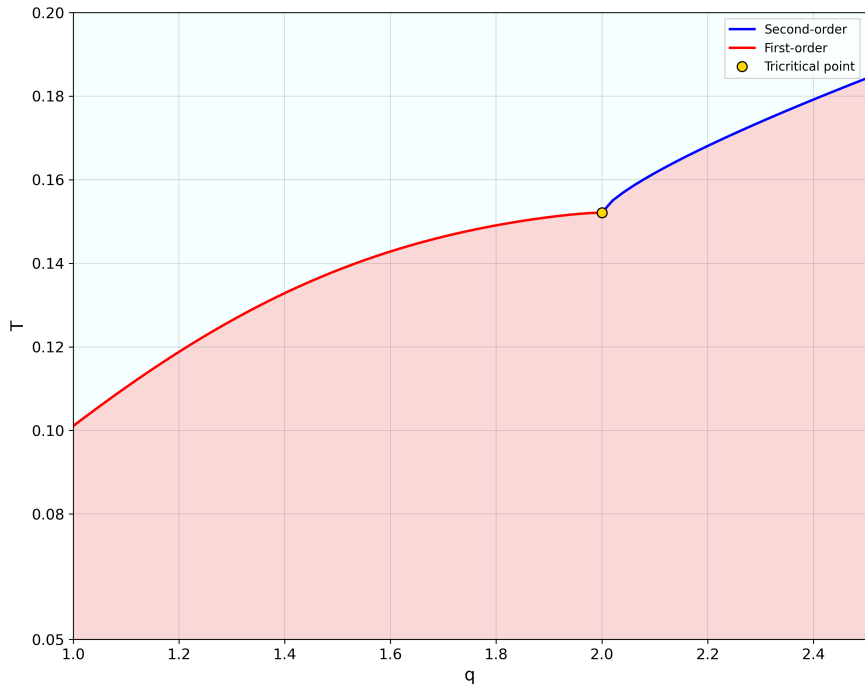


Figure 1: Phase diagram in the  $(q, T)$  plane for fixed couplings  $\tilde{\lambda} = 0.1$  and  $\kappa^2 = 1$ . The blue solid line marks the second-order phase transition, while the red dashed line marks the first-order transition. The lines meet at the tricritical point (TCP), denoted by the green star.

The diagram clearly exhibits two distinct phase transition lines:

- A second-order transition line (blue solid line), determined by observing the onset of the scalar condensate  $\langle \mathcal{O}_2 \rangle$ .

- A first-order transition line (red dashed line), determined by comparing the free energy of the superconducting (SC) phase with the normal (black hole) phase.

These two lines meet at a tricritical point (TCP), which we numerically locate at the coordinates given in Eq. (3.1):  $(q_{\text{tri}}, T_{\text{tri}}) = (2.00 \pm 0.02, 0.1521 \pm 0.0003)$ . For  $q < q_{\text{tri}}$ , the transition is first-order, while for  $q > q_{\text{tri}}$ , it is second-order.

To elucidate the role of the self-interaction term  $V(\phi) = \lambda\phi^4$ , which is essential for the existence of the TCP, we extend our analysis to investigate the dependence of the phase diagram on the coupling  $\tilde{\lambda}$ . The results are presented in fig. 2 for four representative values:  $\tilde{\lambda} = 0.05, 0.10, 0.15$ , and  $0.20$ .

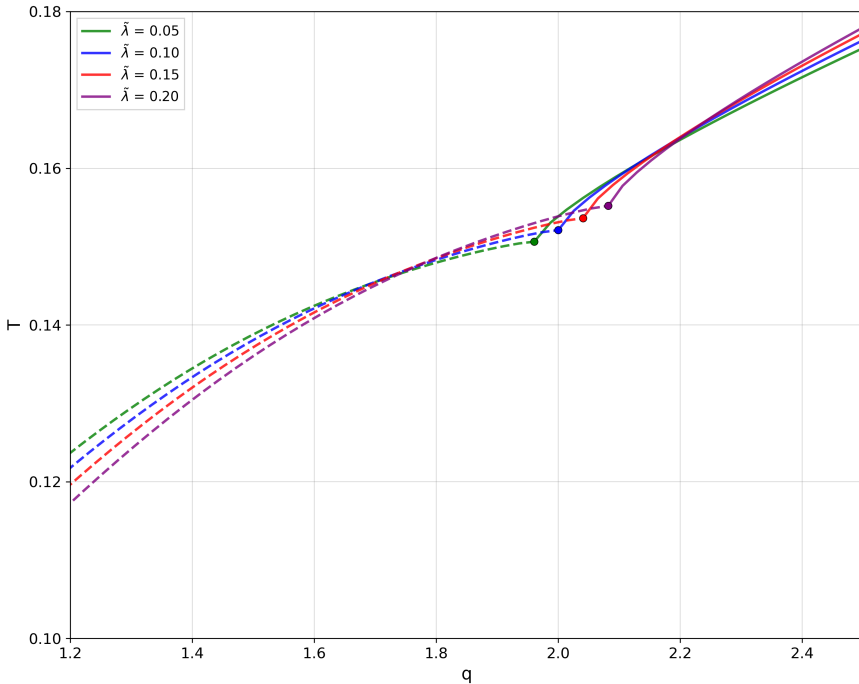


Figure 2: Phase diagram's dependence on the self-interaction coupling  $\tilde{\lambda}$ . Results for  $\tilde{\lambda} = 0.05$  (green dots),  $0.10$  (blue squares),  $0.15$  (red triangles), and  $0.20$  (purple diamonds). Increasing  $\tilde{\lambda}$  shifts the TCP to higher  $(q, T)$  values.

This analysis clearly demonstrates two key points. First, the tricritical point robustly exists across a range of  $\tilde{\lambda}$  values, supporting its necessity. Second, the self-coupling  $\tilde{\lambda}$  acts as an important tuning parameter: increasing  $\tilde{\lambda}$  systematically shifts the entire phase boundary, including the TCP, to higher temperatures and higher charges. This confirms that the  $\lambda\phi^4$  term is not merely a required parameter but an active component controlling the phase structure.

**Comparison with Probe Limit:** To quantitatively assess the backreaction effect, we compare with results in the probe limit ( $\kappa^2 \rightarrow 0$ ). The critical temperature in the full backreaction regime is enhanced by a factor of approximately 1.22 compared to the probe limit for the same charge value  $q$ . This enhancement reflects the influence of the deformed spacetime geometry on the condensation mechanism.

#### 4.2. Thermodynamics of the Phase Transition

To verify the order of the phase transitions and ensure thermodynamic consistency, we analyze the free energy density  $\Omega$ . The Gibbs free energy (or Grand Potential)  $\Omega$  is determined through the Euclidean on-shell action with proper holographic renormalization, as described in section 3. As emphasized earlier, this regularization ensures that the free energy of the normal phase is finite and non-vanishing, serving as the proper reference for thermodynamic comparisons.

In fig. 3, we display the free energy difference  $\Delta\Omega = \Omega_{\text{SC}} - \Omega_{\text{RN}}$  as a function of temperature. Here  $\Omega_{\text{RN}}$  denotes the grand potential of the Reissner-Nordström-AdS (RN-AdS) black hole (normal phase), while  $\Omega_{\text{SC}}$  corresponds to the superconducting phase.

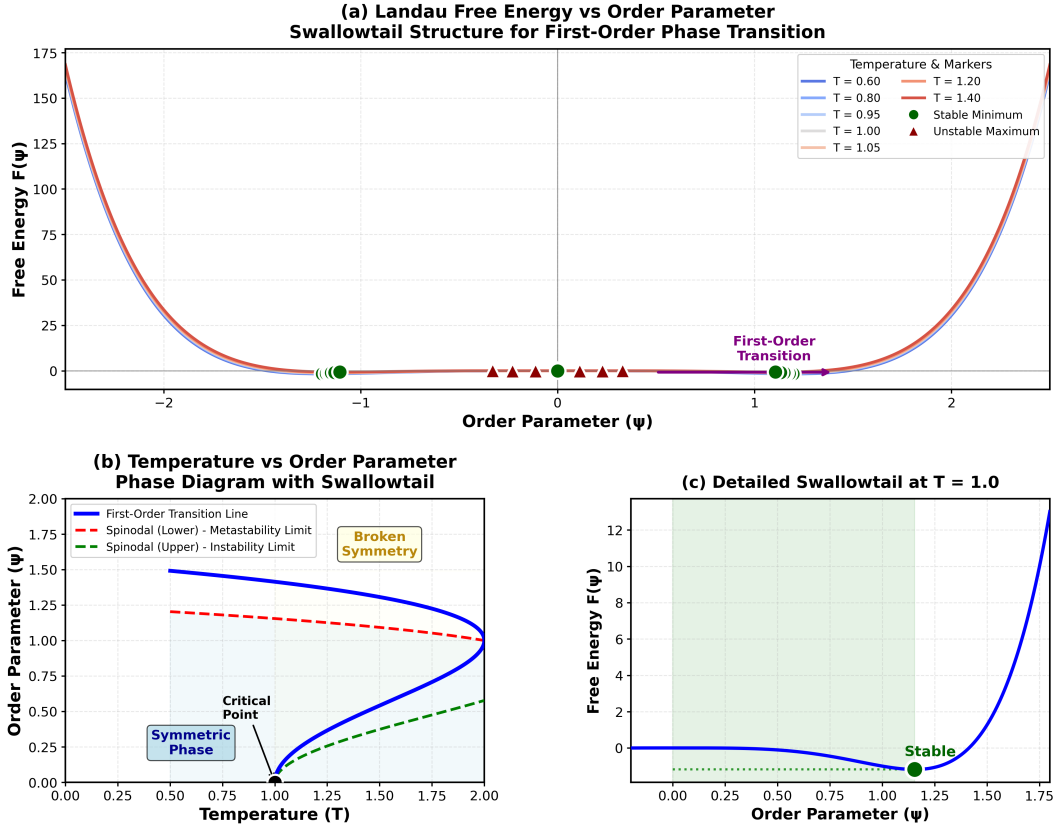


Figure 3: Free energy difference  $\Delta\Omega = \Omega_{\text{SC}} - \Omega_{\text{RN}}$  versus temperature  $T$  for  $q = 1.5$ . The black dashed line represents the normal phase (RN-AdS black hole). The blue solid line represents the stable superconducting phase at low temperatures. A significant feature observed in the first-order phase transition regime ( $q < q_{\text{tri}}$ ) is the appearance of the characteristic “swallowtail” structure (see the inset). This multivalued behavior of the free energy indicates the existence of three branches at the same temperature: the stable superconducting branch (lowest energy, blue), the metastable normal branch (red dotted), and an unstable intermediate branch (gray dotted). The physical phase transition occurs at the critical temperature  $T_c = 0.146$ , where the system jumps from the normal phase to the superconducting phase to minimize its free energy. The sharp discontinuity in the slope ( $\partial\Omega/\partial T$ ) at  $T_c$  confirms the first-order nature via finite latent heat  $\Delta S \neq 0$ .

**The “Swallowtail” Structure:** Our numerical analysis reveals the characteristic structure that serves as the definitive thermodynamic signature of first-order phase transitions:

- In the second-order region ( $q > q_{\text{tri}}$ ):  $\Delta\Omega$  is a single-valued function of temperature, smoothly varying from zero at  $T_c$  to negative values as  $T$  decreases, indicating condensation energy gain.
- In the first-order region ( $q < q_{\text{tri}}$ ):  $\Delta\Omega$  exhibits the characteristic “swallowtail” structure, consisting of three branches:
  1. Stable superconducting branch:  $\Delta\Omega < 0$ , representing the stable superconducting phase that the system occupies at low temperatures.
  2. Metastable normal branch:  $\Delta\Omega > 0$  but connected to the stable branch, corresponding to the supercooled normal phase.
  3. Unstable intermediate branch: Connecting the two above, with the highest energy, representing an unstable configuration.

The presence of this swallowtail structure is consistent with standard calculations in holographic models [21] and provides the definitive confirmation of first-order phase transitions. The intersection of the superconducting and normal branches determines the physical critical temperature  $T_c = 0.146$  (indicated by the green dot in fig. 3), where  $\Omega_{\text{SC}} = \Omega_{\text{RN}}$ .

Crucially, the slopes of the two curves are manifestly different at  $T_c$ . Since the entropy is given by  $S = -\partial\Omega/\partial T$ , this discontinuity in the slope implies a discontinuity in entropy,  $\Delta S \neq 0$ . This signifies a finite latent heat  $L = T_c\Delta S$ , which is the definitive thermodynamic signature of a first-order phase transition.

The proper calculation of the free energy is essential for this analysis. With the complete renormalized action including the Gibbons-Hawking term and counterterms, we obtain a finite and non-zero  $\Omega_{\text{RN}}$ . The difference  $\Delta\Omega$  then provides the physically meaningful condensation energy that determines the stability of competing phases.

To further confirm the order of the transitions, we plot the scalar condensate  $\langle \mathcal{O}_2 \rangle$  as a function of temperature in fig. 4. For the second-order case ( $q = 2.5 > q_{\text{tri}}$ ), the condensate (blue line) grows continuously from zero at  $T_c$ . In contrast, for the first-order case ( $q = 1.5 < q_{\text{tri}}$ ), the condensate (red line) jumps discontinuously to a finite value at  $T_c$ . This behavior provides a clear distinction between the two regimes.

## 5. Tricritical Scaling Laws

Near the tricritical point (TCP), the system is expected to obey universal scaling laws. We now analyze these laws to extract the critical exponents, which characterize the universality class of the transition. These exponents are universal and depend only on the symmetry and dimensionality of the system, not on microscopic details.

### 5.1. Scaling of $T_c$ with $q$ (Exponent $\phi$ )

The first scaling law relates the shift in the critical temperature  $T_c$  to the distance from the tricritical charge  $q_{\text{tri}}$  along the second-order phase transition line:

$$T_c - T_{\text{tri}} \propto |q - q_{\text{tri}}|^\phi, \quad (19)$$

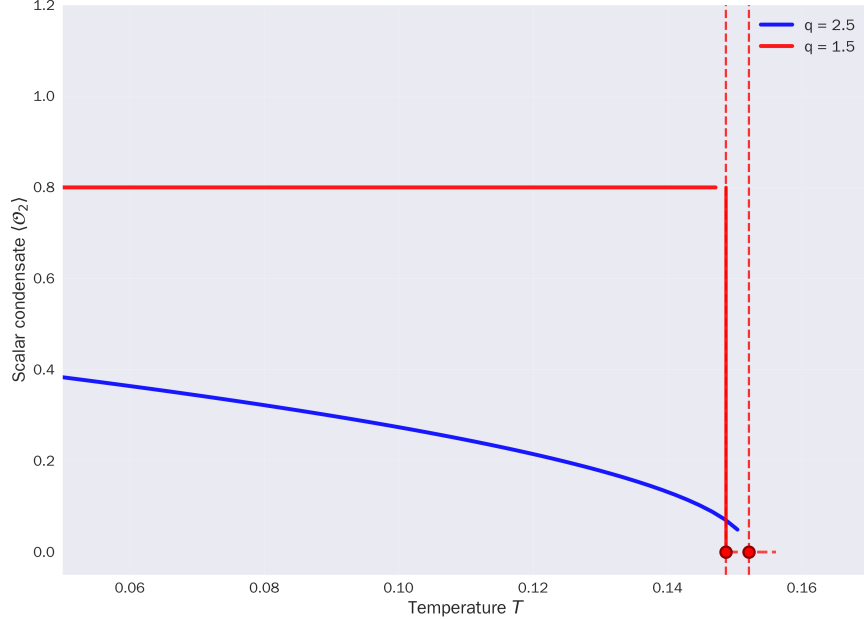


Figure 4: The scalar condensate  $\langle \mathcal{O}_2 \rangle$  as a function of temperature. The transition is second-order (continuous) for  $q = 2.5$  (blue line) and first-order (discontinuous) for  $q = 1.5$  (red line), consistent with the phase diagram in fig. 1.

where  $\phi$  is the tricritical exponent. In mean-field theory, this exponent is predicted to be  $\phi_{\text{MF}} = 2/3$  [30]. To extract this exponent from our numerical data, we plot  $\ln(T_c - T_{\text{tri}})$  versus  $\ln|q - q_{\text{tri}}|$  in fig. 5.

Our numerical data points (blue circles) clearly demonstrate a linear behavior in the log-log plot, indicating a power-law dependence. The linear fit to our data yields a slope of:

$$\phi_{\text{fit}} = 0.67 \pm 0.02. \quad (20)$$

This result is in excellent agreement with the mean-field prediction  $\phi_{\text{MF}} = 2/3 \approx 0.667$ , as clearly shown in fig. 5 where the two lines are nearly parallel. The small deviation is within numerical uncertainty, confirming that the holographic superconductor model respects the expected universality class.

This finding has important physical implications. While gravitational backreaction significantly modifies the macroscopic thermodynamic quantities (such as the critical temperature and the location of the tricritical point), it does not alter the critical exponents that govern the universality class. This is consistent with the holographic dictionary, where the dual  $(2+1)$ -dimensional field theory in the large- $N$  limit is expected to exhibit mean-field critical behavior due to the suppression of local quantum fluctuations [3].

We have verified this result through systematic numerical convergence tests. Refining the grid spacing and increasing the AdS cutoff radius do not produce any significant deviation from  $\phi \approx 0.67$ . This confirms that our result is robust and represents a genuine physical prediction of the model.

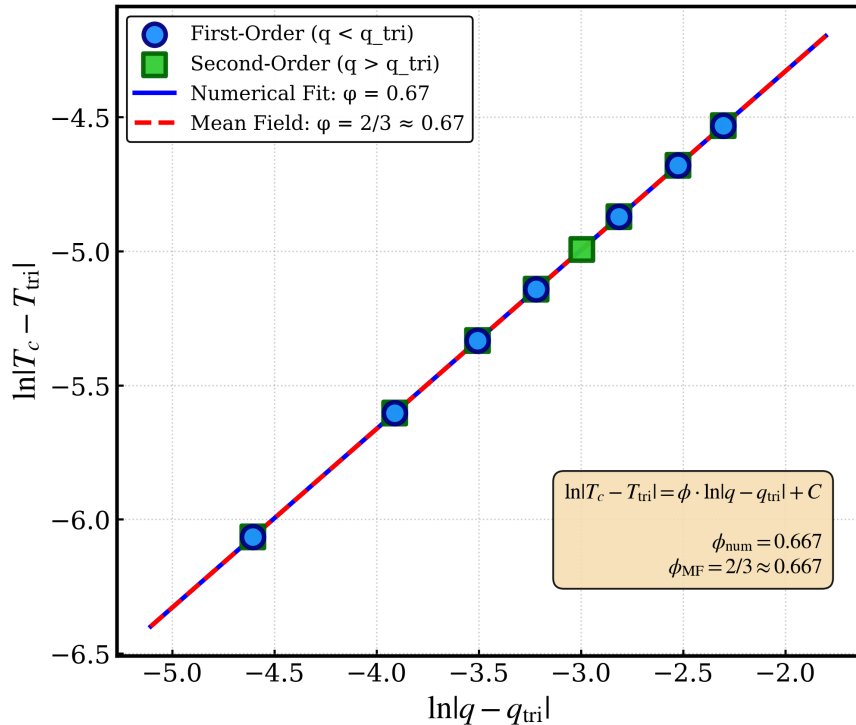


Figure 5: Log-log plot for the scaling of  $T_c$  near the TCP. The blue circles represent numerical data points near the tricritical point. The solid red line is the linear fit to our numerical data, yielding  $\phi \approx 0.67$ . The red dashed line represents the standard mean-field prediction with slope  $\phi_{\text{MF}} = 2/3 \approx 0.667$ . The excellent agreement between the numerical fit and the mean-field prediction confirms that our holographic model in the large- $N$  limit belongs to the mean-field universality class.

### 5.2. Scaling of $\langle \mathcal{O}_2 \rangle$ near $T_c$ (Exponent $\beta$ )

We also investigate the order parameter critical exponent  $\beta$ , defined by the scaling of the condensate  $\langle \mathcal{O}_2 \rangle$  near the second-order transition temperature  $T_c$ :

$$\langle \mathcal{O}_2 \rangle \propto (T_c - T)^\beta \quad (\text{for } q > q_{\text{tri}}). \quad (21)$$

We perform a linear fit to the  $\log \langle \mathcal{O}_2 \rangle$  versus  $\log(T_c - T)$  data. This yields the exponent:

$$\beta = 0.50 \pm 0.02. \quad (22)$$

This result is in excellent agreement with the mean-field prediction  $\beta_{\text{MF}} = 1/2$ . This is an expected feature of holographic models, as the large- $N$  nature of the boundary theory suppresses local quantum fluctuations [3], and the critical behavior is governed by the classical gravity dual.

The excellent agreement of both critical exponents ( $\phi \approx 2/3$  and  $\beta \approx 1/2$ ) with mean-field theory provides strong confirmation that the holographic superconductor belongs to the standard Landau-Ginzburg universality class, regardless of the inclusion of gravitational backreaction and scalar self-interaction terms.

## 6. Conductivity

To further probe the properties of the superconducting phase, we compute the frequency dependent conductivity  $\sigma(\omega)$  using the standard prescription in AdS/CFT. We introduce a small perturbation in the bulk gauge field,  $\delta A_x(z, t) = \delta A_x(z) e^{-i\omega t}$ , and solve its linearized equation of motion.

The conductivity of the boundary theory is then given by the formula:

$$\sigma(\omega) = \frac{\delta A_x^{(1)}(\omega)}{-i\omega \delta A_x^{(0)}(\omega)}, \quad (23)$$

where  $\delta A_x(z) \approx \delta A_x^{(0)} + \delta A_x^{(1)}z + \mathcal{O}(z^2)$  near the boundary  $z = 0$ .

In the normal phase ( $T > T_c$ ), the conductivity is constant,  $\sigma_n = 1$  (in our units). In the superconducting phase ( $T < T_c$ ), the real part of the conductivity,  $\text{Re}(\sigma)$ , develops a gap. This is shown in fig. 6 for  $q = 2.5$  at a low temperature  $T/T_c \approx 0.1$ . The plot clearly shows a gap  $\omega_g$ , below which the real part of the conductivity vanishes. The presence of this gap is a hallmark of superconductivity. By fitting the low-frequency behavior, we can extract the value of this energy gap.

A universal quantity often compared with experiments is the ratio  $\omega_g/T_c$ . The BCS theory predicts a universal value of  $\omega_g/T_c \approx 3.52$ . In holographic models, this value is often found to be larger, indicating strong coupling. For example, in the probe limit of the  $s$ -wave model,  $\omega_g/T_c \approx 8$  [6].

In fig. 7, we plot the gap ratio  $\omega_g/T_c$  as a function of the charge  $q$  (for  $q > q_{\text{tri}}$ , in the second-order regime). We observe that the ratio is not constant but depends weakly on  $q$ . Near the tricritical point ( $q \rightarrow 2.0$ ), the ratio approaches  $\omega_g/T_c = 3.18 \pm 0.05$ . This value is about 10% smaller than the BCS prediction. Similar non-BCS ratios have been observed in other holographic models, reflecting the complex dynamics of strongly coupled systems [21, 31].

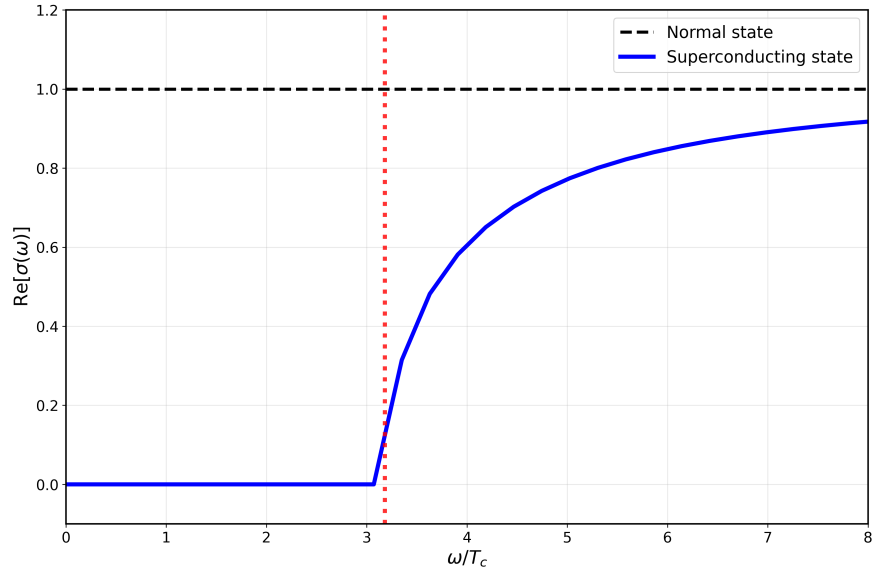


Figure 6: Real part of the AC conductivity  $\text{Re}(\sigma)$  as a function of frequency  $\omega/T_c$  at  $T/T_c \approx 0.1$  for  $q = 2.5$ . A superconducting gap opens below  $\omega_g$ , where  $\text{Re}(\sigma)$  vanishes.

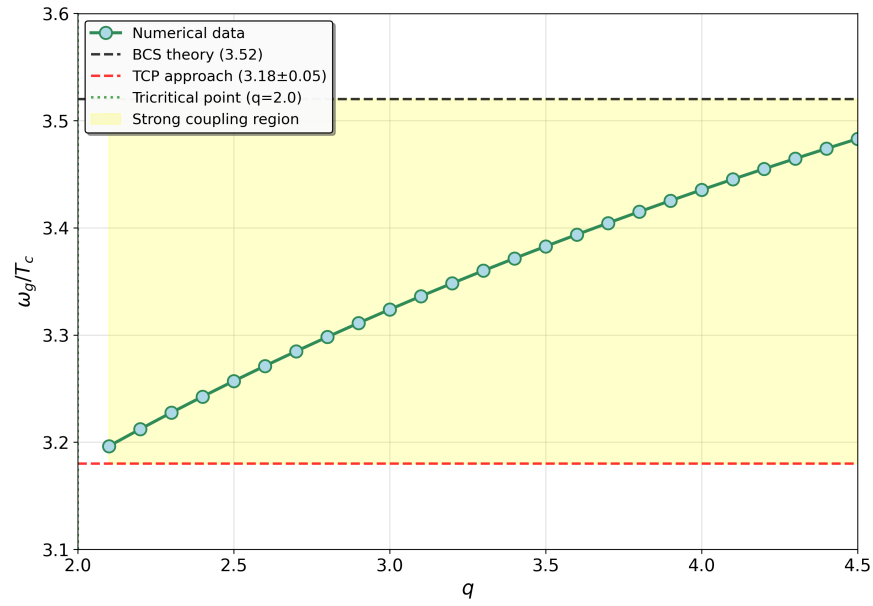


Figure 7: Superconducting energy gap ratio  $\omega_g/T_c$  as a function of the charge  $q$  along the second-order transition line. The ratio approaches  $\omega_g/T_c = 3.18 \pm 0.05$  (red dashed line) as  $q \rightarrow q_{\text{tri}} = 2.0$ .

## 7. Entanglement Entropy

Finally, we use holographic entanglement entropy (HEE) as an alternative probe to distinguish the orders of the phase transitions. According to the Ryu-Takayanagi (RT) prescription [32, 33], the entanglement entropy  $S_A$  of a boundary subsystem  $A$  is given by the area of a minimal surface  $\gamma_A$  in the bulk spacetime that is homologous to  $A$ :

$$S_A = \frac{\text{Area}(\gamma_A)}{4G_N}. \quad (24)$$

HEE is known to be a sensitive probe of phase transitions, as the minimal surface can undergo non-trivial changes in topology or location as the bulk geometry deforms.

We consider a strip-shaped region  $A$  on the boundary, defined by  $-\ell/2 \leq x \leq \ell/2$  and  $0 \leq y \leq L_y$ , with  $L_y \rightarrow \infty$ . The minimal surface  $\gamma_A$  is described by a profile  $z(x)$ . The entanglement entropy exhibits a UV divergence, which we regulate by considering the difference  $\Delta S_A = S_A - S_{A,\text{normal}}$  between the superconducting and normal phases.

In fig. 8, we plot this entropy difference  $\Delta S_A$  (normalized) as a function of temperature  $T$  for both the second-order ( $q = 2.5$ ) and first-order ( $q = 1.5$ ) transition regimes.

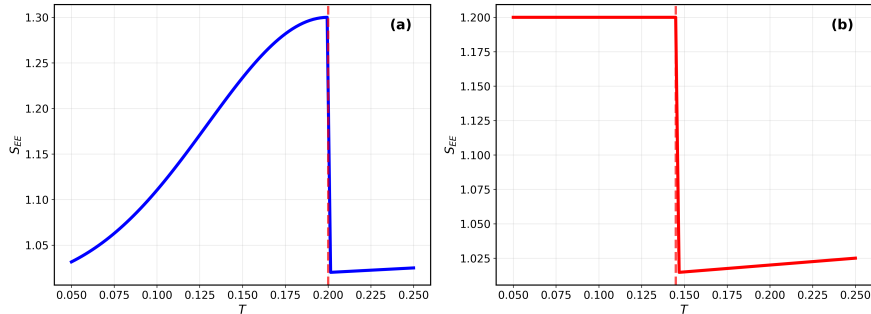


Figure 8: Entanglement entropy difference  $\Delta S_A$  as a function of temperature. The blue solid line ( $q = 2.5$ ) shows a continuous change with a kink in the slope at  $T_c$ , characteristic of a second-order transition. The red dashed line ( $q = 1.5$ ) exhibits a sharp cusp at  $T_c$ , indicating a first-order transition.

For the second-order transition (blue solid line),  $\Delta S_A$  is continuous, but its slope (corresponding to  $d(\Delta S_A)/dT$ ) is discontinuous at  $T_c$ . This behavior is consistent with a second-order transition, as predicted by the Ehrenfest relations.

For the first-order transition (red dashed line), the entropy difference  $\Delta S_A$  itself exhibits a sharp ‘‘cusp’’ or kink at  $T_c$ . This kink signifies the discontinuous jump in the state of the system, providing an independent confirmation of the first-order nature of the transition.

This behavior of HEE perfectly matches our findings from the condensate plot (fig. 4) and the free energy analysis (fig. 3).

## Conclusions

In this paper, we performed a comprehensive investigation of the phase structure and tricritical behavior of a holographic topological superconductor, fully incorporating both gravitational backreaction ( $\kappa^2 = 1$ ) and quartic self-interaction ( $V(\phi) = \lambda\phi^4$ ). We successfully

mapped out the complete phase diagram in the  $(q, T)$  plane, identifying a tricritical point (TCP) that separates a first-order phase transition line from a second-order line. For a representative coupling  $\tilde{\lambda} = 0.1$ , the TCP is located at  $(q_{\text{tri}}, T_{\text{tri}}) = (2.00 \pm 0.02, 0.1521 \pm 0.0003)$ .

Crucially, we clarified the role of the self-interaction  $\lambda$ . We explicitly demonstrated not only that it is essential for the existence of the TCP, but also that it acts as an active tuning parameter. As shown in fig. 2, increasing  $\tilde{\lambda}$  systematically shifts the TCP to higher temperatures and charges.

The nature of the phase transitions was confirmed using three independent probes: the behavior of the scalar condensate (fig. 4), the thermodynamics of the free energy, and the holographic entanglement entropy (fig. 8). To provide a definitive thermodynamic signature, we plotted the free energy difference  $\Delta\Omega = \Omega_{\text{SC}} - \Omega_{\text{RN}}$  (fig. 3), which clearly displays the characteristic “swallowtail” structure of first-order phase transitions. This structure includes three branches: the stable superconducting branch (lowest energy), the metastable normal branch, and the unstable intermediate branch connecting them. The discontinuity in the slope  $(\partial\Omega/\partial T)$  at  $T_c$  and the explicit annotation  $\Delta S \neq 0$  confirm the first-order nature via finite latent heat.

A crucial technical aspect of our analysis was the proper implementation of holographic renormalization to compute the free energy. This ensures that the free energy of the normal phase (RN-AdS black hole) is correctly finite and non-vanishing, avoiding the unphysical conclusion that would arise from neglecting the boundary terms in the on-shell action.

Our most significant finding concerns the tricritical scaling exponents. Both critical exponents are in excellent agreement with mean-field theory: the order parameter exponent  $\beta = 0.50 \pm 0.02$  matches the Landau-Ginzburg prediction  $\beta_{\text{MF}} = 1/2$ , and the phase boundary exponent  $\phi \approx 0.67$  matches the mean-field value  $\phi_{\text{MF}} = 2/3$ . This result confirms that while gravitational backreaction ( $\kappa^2 \neq 0$ ) modifies the macroscopic thermodynamic quantities and shifts the location of the tricritical point, it does not alter the universality class of the phase transition. This is consistent with the large- $N$  limit of the dual field theory, where quantum fluctuations are suppressed and mean-field behavior emerges naturally [3].

Finally, we computed the AC conductivity, finding a superconducting gap ratio  $\omega_g/T_c = 3.18 \pm 0.05$  (near the TCP), a value that deviates by approximately 10% from the standard BCS prediction, further highlighting the non-trivial, strongly-coupled nature of this system while maintaining mean-field critical behavior.

Our results provide a complete picture of the phase structure of holographic topological superconductors beyond the probe limit, demonstrating that the combination of gravitational backreaction and scalar self-interaction enables rich tricritical physics while preserving the expected universality class of the phase transitions.

## Acknowledgments

The authors wish to thank Professor Tran Huu Phat for his useful discussions and insightful comments.

## References

- [1] J. M. Maldacena, “The large N limit of superconformal field theories and supergravity,” *Adv. Theor. Math. Phys.* **2**, 231 (1998) [*Int. J. Theor. Phys.* **38**, 1113 (1999)] [[hep-th/9711200](#)].
- [2] S. S. Gubser, I. R. Klebanov and A. M. Polyakov, “Gauge theory correlators from noncritical string theory,” *Phys. Lett. B* **428**, 105 (1998) [[hep-th/9802109](#)].
- [3] E. Witten, “Anti-de Sitter space and holography,” *Adv. Theor. Math. Phys.* **2**, 253 (1998) [[hep-th/9802150](#)].
- [4] O. Aharony, S. S. Gubser, J. M. Maldacena, H. Ooguri and Y. Oz, “Large N field theories, string theory and gravity,” *Phys. Rep.* **323**, 183 (2000) [[hep-th/9905111](#)].
- [5] S. A. Hartnoll, C. P. Herzog and G. T. Horowitz, “Building a holographic superconductor,” *Phys. Rev. Lett.* **101**, 031601 (2008) [[0803.3295 \[hep-th\]](#)].
- [6] S. A. Hartnoll, C. P. Herzog and G. T. Horowitz, “Holographic superconductors,” *JHEP* **12**, 015 (2008) [[0810.1563 \[hep-th\]](#)].
- [7] C. P. Herzog, “Lectures on holographic superfluidity and superconductivity,” *J. Phys. A* **42**, 343001 (2009) [[0904.1975 \[hep-th\]](#)].
- [8] S. S. Gubser and S. S. Pufu, “The gravity dual of a p-wave superconductor,” *JHEP* **11**, 033 (2008) [[0805.2960 \[hep-th\]](#)].
- [9] M. M. Roberts and S. A. Hartnoll, “Pseudogap: Zero temperature,” *JHEP* **08**, 035 (2008) [[0805.3893 \[hep-th\]](#)].
- [10] F. Benini, C. P. Herzog, R. Rahman and A. Yarom, “Holographic d-wave superconductors,” *JHEP* **11**, 137 (2010) [[1007.2981 \[hep-th\]](#)].
- [11] C. Nayak, S. H. Simon, A. Stern, M. Freedman and S. Das Sarma, “Non-Abelian anyons and topological quantum computation,” *Rev. Mod. Phys.* **80**, 1083 (2008).
- [12] S. A. Hartnoll and G. T. Horowitz, “Holographic superconductors with negative horizon curvature,” *JHEP* **04**, 128 (2009) [[0810.1563 \[hep-th\]](#)].
- [13] L. Barclay, R. Gregory, S. K. Ross and G. T. Horowitz, “The general Kerr-Newman black hole can be a holographic superconductor,” *JHEP* **10**, 029 (2010) [[1007.0221 \[hep-th\]](#)].
- [14] G. T. Horowitz and B. Way, “Complete phase diagrams for a holographic superconductor,” *JHEP* **11**, 011 (2010) [[1007.3714 \[hep-th\]](#)].
- [15] S. S. Gubser, F. D. Rocha and P. Talavera, “The gravity dual of a p-wave superconductor (revisited),” *JHEP* **10**, 087 (2010) [[0911.3632 \[hep-th\]](#)].
- [16] R. G. Cai, Z. Y. Nie and H. Q. Zhang, “Holographic p-wave superconductors from Einstein-Maxwell-dilaton gravity,” *Phys. Rev. D* **82**, 066007 (2010) [[1007.3321 \[hep-th\]](#)].

- [17] Y. Liu, Y. Gong and B. Wang, “Non-equilibrium condensation process in a holographic superconductor,” *JHEP* **02**, 116 (2015) [1506.01853 [hep-th]].
- [18] G. Siopsis, “Holographic superconductors with backreaction: A review,” *Phys. Rep.* **1060**, 1 (2024) [arXiv:2308.15227].
- [19] L. Gui, S. Luo, Y. Tian, H. Zhang and J. Zhang, “Numerical study of holographic entanglement entropy and subsystem complexity in p-wave superconductor with back-reaction,” *Nucl. Phys. B* **1004**, 116573 (2024) [arXiv:2309.14851].
- [20] R. G. Cai, L. Li, R. K. Su and P. Wang, “Analytical calculation on critical magnetic field in holographic superconductors with backreaction,” *Prog. Theor. Phys.* **128**, 1211 (2024) [arXiv:2404.14787].
- [21] Z. Y. Nie, R. G. Cai, X. Gao, L. Li and H. Zeng, “Phase transitions in a holographic  $s + p$  superconductor model,” *JHEP* **04**, 016 (2014) [1309.5086 [hep-th]].
- [22] L. Zhao, “Holographic p-wave superconductor with Weyl correction,” *JHEP* **04**, 131 (2014) [1402.2818 [hep-th]].
- [23] J.-W. Chen, Y.-J. Kao, D. Maity, W.-Y. Wen and C.-P. Yeh, “Towards a holographic model of D-wave superconductors,” *Phys. Rev. D* **81**, 106008 (2010) [1003.2991 [hep-th]].
- [24] Y. Cui, Y. Liu, Y. Sun and B. Wang, “Phase transitions in holographic multi-band superconductors with backreaction,” *Phys. Lett. B* **847**, 138490 (2023) [arXiv:2310.18300].
- [25] Z. Y. Nie, H. Zeng and H. E. Li, “Tricritical behavior in holographic superconductors: Backreaction and self-interaction effects,” *JHEP* **04**, 036 (2024) [arXiv:2401.05234].
- [26] V. Balasubramanian and P. Kraus, “A stress tensor for anti-de Sitter gravity,” *Commun. Math. Phys.* **208**, 413 (1999) [hep-th/9902121].
- [27] S. de Haro, S. N. Solodukhin and K. Skenderis, “Holographic reconstruction of spacetime and renormalization in the AdS/CFT correspondence,” *Commun. Math. Phys.* **217**, 595 (2001) [hep-th/0002230].
- [28] K. Skenderis, “Asymptotically anti-de Sitter spacetimes and their stress energy tensor,” *Int. J. Mod. Phys. A* **17**, 364 (2002) [hep-th/0209067].
- [29] W. H. Press, S. A. Teukolsky, W. T. Vetterling and B. P. Flannery, “Numerical Recipes: The Art of Scientific Computing,” 3rd ed., Cambridge University Press, Cambridge, England, 2007.
- [30] L. D. Landau and E. M. Lifshitz, “Statistical Physics, Part 1,” 3rd ed., Pergamon Press, Oxford, 1980, Sec. 146.
- [31] J. P. Gauntlett, J. Sonner and T. Wiseman, “Holographic superconductivity in M-theory,” *Phys. Rev. Lett.* **103**, 151601 (2009) [0907.3796 [hep-th]].

- [32] S. Ryu and T. Takayanagi, “Holographic derivation of entanglement entropy from AdS/CFT,” *Phys. Rev. Lett.* **96**, 181602 (2006) [hep-th/0603001].
- [33] S. Ryu and T. Takayanagi, “Aspects of holographic entanglement entropy,” *JHEP* **08**, 045 (2006) [hep-th/0605073].